IEEE Access
Multidisciplinary ⋮ Rapid Review ⋮ Open Access Journal

Received 16 January 2023, accepted 24 January 2023, date of publication 1 February 2023, date of current version 7 February 2023.

Digital Object Identifier 10.1109/ACCESS.2023.3241361

RESEARCH ARTICLE

In-Situ Estimation of Bolt Clamping Force by Utilization of Its Effects on Flexural Vibration Propagation

WANSEUNG KIM[1], YEONUK SEONG[1], JONGSEONG KIM[2], AND JUNHONG PARK[1]

[1]Department of Mechanical Engineering, Hanyang University, Seoul 04763, Republic of Korea
[2]Commercial Vehicle Production Engineering Team, Hyundai Motor Group, Wanju-gun, Jeollabuk-do 55322, Republic of Korea

Corresponding author: Junhong Park (parkj@hanyang.ac.kr)

This work was supported by the National Research Foundation of Korea (NRF) funded by the Korea Government through MSIT (Solution Development for Non-Destructive Evaluation Challenge Based on Data Science) under Grant 2021M2E6A1084690.

ABSTRACT After a bolt assembling process, non-destructive identification of the clamping force is important to minimize unexpected failure of the assembled joint structures. For in-situ inspection for every parts, a detachable device which allows generation and detection of vibration propagation was proposed in this study. Tone burst excitation was transmitted through the bolted-joint structure. The vibration propagation characteristics depended on the clamping force. With an increase in the clamping force, the surface vibration propagation speed increased. The vibration magnitude decreased due to increasing constraint. A band-pass filter was used to remove noise component. The filtered vibration propagation responses were used in convolutional long short-term memory (CLSTM) training. The performance of CLSTM model was verified through comparison with actual clamping force. With minimal physical influence on the assembled parts, the clamping force of bolted-joint was measured using the surface vibration propagation characteristics.

INDEX TERMS Flexural vibration, clamping force, deep learning.

I. INTRODUCTION

Bolted joints are widely used to connect separate structures owing to their efficiency during production process. The reliability of the joint depends on the applied clamping force. To secure the structural integrity with minimal possibility of failure after production, it is required to inspect the assembled status of the joints. The inspection should be performed without any permanent mark with less influence on task time. For application to manufacturing process, it is advantageous to inspect clamping force using the mechanical characteristics of joint.

During bolt tightening, 90 percent of the mechanical energy input from the tool is dissipated by friction at the contact surface and the thread [1]. The remaining energy is converted to the potential elastic energy from longitudinal elongation of the shank. This elastic elongation induces the clamping force of the bolted-joint structure. Fundamental principle for estimating the clamping force is that bolt tightening is performed by the torque or angle control. Firstly, clamping force is estimated from the applied torque [2]. In this method, tightening parameters such as fastening speed, temperature and humidity affect the friction coefficient which causes large variations on estimating result. Secondly, the angle control method utilizes the linear relationship between the rotation angle and bolt tension [3]. In comparison with the torque control method, it shows a better performance on the generation of the uniform clamping force.

Insufficient clamping force leads to the bolt loosening and causes structural failure during operation. The bolt loosening occurs rapidly right after fastening by creep and slippage. Temperature variation is the main causes of accelerated bolt loosening in the aluminum-composite bolt joint [4]. At high temperature, stiffness in the axial direction increases. The allowable load value of high temperature becomes lower than low temperature [5]. The influence of temperature was investigated by using the angular deformation [6]. Basava and Hess investigated the change in axial force of the

The associate editor coordinating the review of this manuscript and approving it for publication was Prakasam Periasamy.

single-bolt assembly by the longitudinal vibration [7]. The low preload and high-level vibration induce significant bolt loosening.

To secure uniform production quality of jointed part, it is required to monitor the clamping force. In case of the direct measurement, load cell or strain gauge should be installed prior to the bolt fastening. Grzejda and Parus [8] monitored the clamping force of multi-bolted connection systems based on resistance strain gauges. There is a difficulty on application to the production process since the strain gauges installation to the bolt is required prior to measurement. A method using mechanical properties of bolt structure is required to measure the clamping force after fastening. For the assembled part, estimation of the clamping force without separation or deformation has been a topic of research [9]. To estimate the clamping force indirectly, vibration and sound generation during the tightening process were used as a fastening characteristics [10]. The wave propagation in the contact surface was also used to evaluate the clamping force. Natural frequency was measured by applying an impact to the bolt head. The first natural frequency changed according to the clamping force [11]. Bolt axial force measurement using ultrasound is widely used for indirect characterization [12]. Time of flight (TOF) was calculated using the ultrasonic waves generated at the bolt head. The amount of elongation of the bolt indicated the clamping force. Although the ultrasonic method shows a high level of accuracy, there is a disadvantage that the process of machining the bolt head must be performed in advance. To monitor the loads in bolts and cooperating elements non-destructively, a self-excited acoustic system was suggested [13]. Using the relationship between wave propagation and the frequency of the system, the load, displacement and frequency behavior curves were determined. Surface vibration propagation and reflection depending on the bolt tension was also investigated [14]. In the reflected wave, the average vibration amplitude increased with the increasing tensile force. The vibration energy attenuation was used to measure the bolt clamping force. A numerical model was presented to simulate the effects of the clamping force on the wave energy loss in the contact. Piezoelectric transducer based electromechanical impedance technology was studied to monitor the looseness of flange bolt [15]. Index of conductance correlation difference under the noise and looseness conditions was suggested in this study.

It is important to secure enough clamping force in the vehicle wheel attachment to minimize heavy wheel separation and consequent serious accident during road transport [16], [17]. The effect of oscillatory movements in bus suspension on the wheel joint detachment was analyzed [18]. Failure mechanism of the fastener was investigated using various force sensors including strain gauges, capacitors, and piezo-resistive sensors [19]. Joint state is also an important subject of research in segmental tunnel linings. Gong et al. [20] developed a hydrodynamic 3D model that numerically simulate the circumferential joint leaks.

As a state-of-the-art approach, deep learning and vision based method has been studied to monitor the clamping force. The two approaches are used to overcome the sensitive change according to the noisy environment. A convolutional neural network (CNN) model was suggested to measure the amount of bolt loosening when an impact occurs by acquiring the acoustic signal generated according to percussion [21]. The rotating feature was used as a feature of CNN [22]. By attaching a coded marker to the bolt, the image was decoded to monitor the rotation between the bolt and nut. The edge detection allowed determination of the rotating component. The bolt loosening was predicted using the proportional relationship between the rotation amount and the clamping force. A visual barcode marker was suggested to obtain the rotation of highly symmetrical structures [23]. This marker robustly extracted the relative angle of the bolt and nut. At vision approach, the signal processing for 3D data of the whole train body caused decreasing efficiency of fault detection. Sun et al. [24] improved accuracy through CNN using extracted train's key components based on binocular vision.

With the purpose for application to monitor the clamping condition in the production process, a device with capability of consistent attachment and easy detachment without any permanent mark on the testing parts is required. In this study, vibration transfer through the testing parts was used for clamping force identification. The device induce the forced excitation on the surface of the clamped parts. The vibration was measured at the specific distance from the excitation location. The effect of clamping force was monitored from the difference on the vibration transfer characteristics. The vibration response was used as an input of transposed convolution layer for expanding data to the unmeasured range. The whole dataset was used in the feature of CLSTM. The performance of deep learning model was verified through comparison with the actual clamping force measured by the load cell. The proposed bolted joint status estimation system allows easy installation and rapid evaluation without permanent modification of the test structure.

II. EFFECT OF CLAMPING FORCE ON FLEXURAL VIBRATION

A. CONCEPT FOR VIBRATION SENSING AND CLAMPING FORCE CHARACTERISTICS ACQUISITION

Figure 1 shows a schematic of the clamping force sensing device. The device consisted of two legs, one for the transmission of ultrasonic wave and the other for sensing the structural vibration. An elongated body was devised to avoid unintended flanking paths. In the generator part, a piezoelectric element (NAC 2013 5 × 5, Noliac, Inc.) was used to induce the vibration transmission. In the receiver part, an accelerometer (7259 B, Endevco, Inc.) was used to measure the vibration passed through the wheel surface and nut. Neodymium magnets were placed in the cylindrical jig at the bottom of device for consistent contact with the nut head. The device was attached to the wheel assembly by pressing

the top handle. Compressive force to the nut increased in proportional to the displacement multiplied by the spring stiffness. When the compressive force and the magnetic force were in balance, the cylindrical jig was attached tightly to the nut. It was designed to maintain the contact condition consistently and enabled the transmission of an enough excitation energy required for characterization of the clamping force effect. In case the device was not in strong contact with the surface, the amount of vibration energy transferred to the wheel surface changed because of structural instability. To improve reproducibility and reliability, the identical compressive force was applied in repeated measurements.

After attaching the equipment so that the bolt joint was in the middle of the leg, the wheel surface was excited. The vibration wave passed through the nut. The excitation input voltage was made from the function generator (33500B, Agilent). Gaussian-shaped tone burst waveform (50 kHz) was designed to operate in a limited frequency range. The generated voltage was sent to the conditioning amplifier (E4114B1, Dytran). Amplified signal was input to the piezo exciter having resonant frequency of 500 kHz. The generated vibration transfer through the wheel surface. The wave past the nut was detected by the accelerometer on the opposite side. The vibration response was acquired using an oscilloscope (DSO-X-4043A, Agilent, Inc.) at a sampling rate of 250 MHz. To measure the actual clamping force value, a washer-type force sensor (KMR $\sim$ 300kN, HBM) was attached between the bolt and the nut structure. The testing structure consisted of aluminum 6061 alloy plate, SCM435 alloy steel bolt and SUS304 stainless steel nut. The bolt head size was M18 and length was 60mm. The vibration transmission path is detailed in Figure 2.

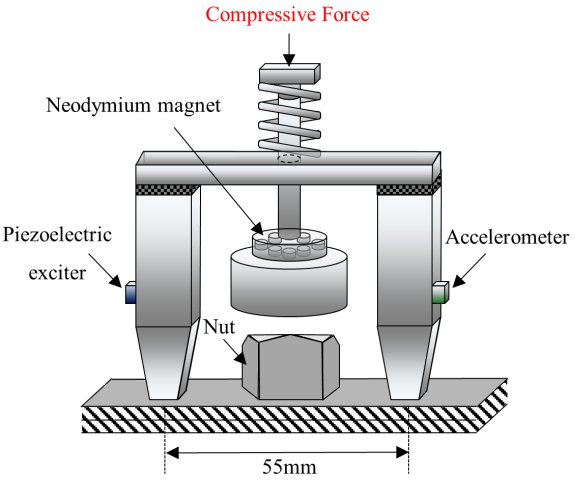

FIGURE 1. Schematic of device using probe legs to measure the TOF for identification of the clamping force.

B. FLEXURAL VIBRATION PROPAGATION THROUGH BOLTED JOINT SURFACE

To observe the vibration wave transfer characteristics, the piezoelectric exciter and accelerometer were directly fixed to the wheel surface. The vibration response was measured by the accelerometer along the arced path as shown in Figure 3.

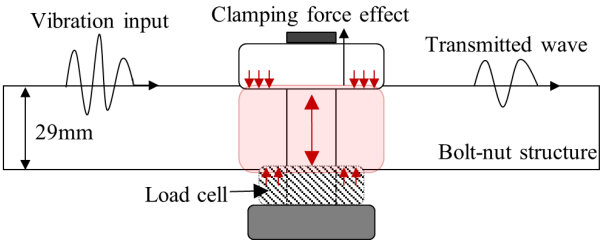

FIGURE 2. Schematic system overview for inspection of blot clamping force using vibration transmission.

The generated flexural vibration from the piezoelectric exciter proceeded along the periphery of the wheel surface. Figure 4 shows the vibration responses according to the distance from the exciter. For the first wave measured by accelerometer, the magnitude decreased and the arrival time delayed with the distance from the piezoelectric exciter with attenuated amplitude. This dependence of the propagation weakened over time because various transmission paths were combined at remoter locations. The measured vibration at each position showed the dispersion characteristics. At close locations from the exciter, the measured vibration maintained the waveform of the tone burst. At measurement point of the device leg, the response showed multiple paths of wave propagation. To obtain a structural vibration feature reflecting only the clamping force characteristics, the fastest two waves were acquired. It was used in the deep learning input after application of the several signal processing.

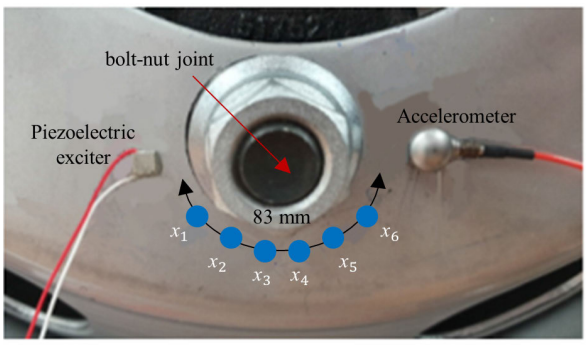

FIGURE 3. Experimental setup to identify the surface vibration transfer on the bolted joint.

C. EFFECT OF CLAMPING FORCE ON FLEXURAL VIBRATION

The behavior of the transverse vibration was analyzed under the axial force from the joint. When the beam is influenced by tensile or compressive force, the flexural vibration propagation follows [25]:

$$EI\frac{\partial^4 w}{\partial x^4} - T\frac{\partial^2 w}{\partial x^2} - \rho A\frac{\partial^2 w}{\partial t^2} = 0, \tag{1}$$

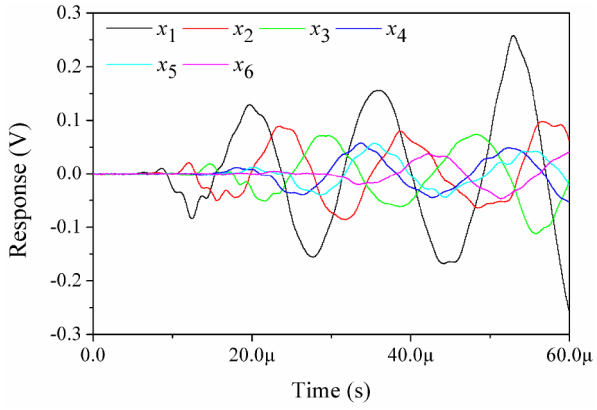

FIGURE 4. Variation of vibration with the wave propagation on the bolted joint surface.

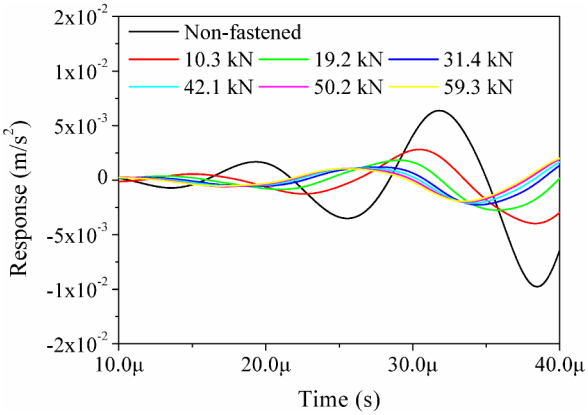

FIGURE 5. Vibration response measured for the clamping force from 0 to 60 kN.

where c is the Young's modulus, I is the second moment area, T is the axial load, ρ is the mass density, A is the cross-sectional area, w is transverse displacement, x is the distance from the end.

The harmonic solution of the flexural vibration equation is given as

$$w(\zeta) = A_1 \sinh(Vx) + A_2 \cosh(Vx) + A_3 \sin(Wx) + A_4 \cos(Wx), \tag{2}$$

where V and W are defined as

$$V, W = \sqrt{\left(\pm\frac{T}{2EI}\right) + \sqrt{\left\{\left(\frac{T}{2EI}\right)^2 + \omega^2 \frac{\rho A}{EI}\right\}}}. \tag{3}$$

Here, ω is the circular natural frequency of the harmonic vibration.

During the fastening of the bolts, axial force acting on the wheel assembly increases. Both flexural wavelength V and W were determined by the axial force according to equations (1) and (3). One was proportional and the other was inversely proportional to the axial force. The clamping force induced a stiffness effect on the transverse direction. The stiffness increased with the larger clamping force.

D. INFLUENCE OF CLAMPING FORCE ON VIBRATION PROPAGATION

Figure 5 shows the influence of the clamping force on the flexural vibration propagation. The experiment was conducted while changing the clamping force from 10 to 60 kN. Speed of the flexural wave showed a continuous increase with the increasing clamping force. The strong fastening process induced a low flexural wavelength component which lead to an increase in speed of the wave. Amplitude of the flexural vibration response also decreased. High effective stiffness induced reduction of the flexural vibration magnitude by energy absorptions. The tendency of wave speed and magnitude is detailed in Figure 6.

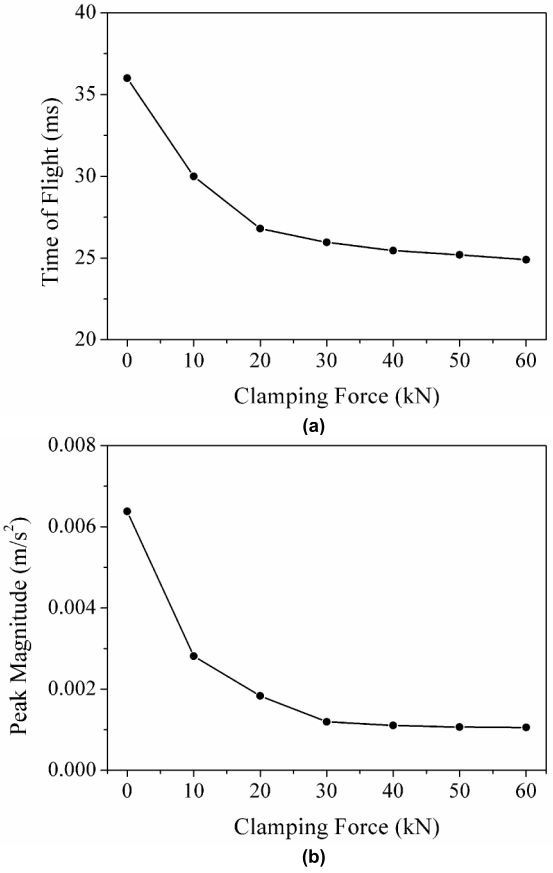

FIGURE 6. Effect of clamping force on the wave propagation properties: (a) the TOF and (b) the peak magnitude.

III. DEEP LEARNING METHODOLOGY

A. DATA ACQUISITION AND PRE-PROCESSING

Data acquisitions were carried out for the clamping forces of 0, 10, 20, 30, 40, 50, and 60 kN. The vibration responses for the data sets were acquired through iterative experiments with the variations of the clamping force. Total 16 data sets were obtained for each clamping force. The data sets were divided into training and test sets at a 4:1 ratio. The measured

vibration responses contained noise components owing to wave reflections at different frequency ranges. A band-pass filter was used to extract only the frequency band components of the excitation. The band-pass filter was performed in the frequency range from 45 to 55 kHz. A smooth curve after the application of the filter was advantageous for shortening the time required to form a deep learning model and for more effective convergence.

B. TRANSPOSED CONVOLUTION

The time series of the unmeasured range was predicted using the characteristics of the measured data. In order to expand range to unmeasured clamping forces, a transposed convolution model was proposed. The transposed convolution is an up-sampling method that can convert smaller resolution into the higher resolution. In trained model, the measured clamping force by the load cell was used in the input of transposed model. The measured time series was also used in the final output of the transposed model. The model architecture was composed of 6 transposed layer stack. The stack has an advantage of nonlinear learning effect. After learning was complete, new class (71 class consist of 1 to 70 kN in 1 kN intervals) were used as an input of the model to predict. The predicted time series was acquired corresponding to each clamping force. A total of 852 training data sets were generated for the CLSTM network.

C. CLSTM METHOD

The pre-processed vibration responses for each clamping force were used as the input of the double 1-D convolutional neural network. The clamping force immediately after tightening was used to exclude loosening by the bolt embedding process. The input size was 10000. The kernel size of each convolutional layer was 5. The pooling size was 8 with max pooling strategy. This process send the time-dependent amplitude data to the long short-term memory (LSTM) layer with less spatial size without information loss.

The LSTM neural network is the improved version of a recurrent neural network (RNN) for classification and prediction based on the time-series data. In RNN, the backpropagation information is not delivered to the hidden-state at the front of the sequence. Thus, the vanishing gradient problem occurs. On the other hand, LSTM overcome the problem by introduction of a cell and gate. It deletes unnecessary memory and remember relatively important memory at each time step. Figure 7. shows the flow and architecture of the neural network process.

When the input values are given, the LSTM cell determine which information is selected. The cell is made up of a forget gate and an input gate. The selection process of LSTM is as follows [26]:

$$f_t = \sigma(W_f[h_{t-1}, x_t] + b_f), \tag{4}$$
$$i_t = \sigma(W_i[h_{t-1}, x_t] + b_i), \tag{5}$$
$$g_t = \tanh(W_g[h_{t-1}, x_t] + b_g), \tag{6}$$

where f_t is a forget gate for removing unnecessary data. i_t and g_t are the input gates to store the new information. They are sum and product of previous time hidden state h_{t-1}, current time vibration input x_t, weights W_f, W_i, W_g and biases b_f, b_i, b_g. The sigmoid function converts from 0 to 1 according to importance. The hyperbolic tangent function converts from -1 to 1 which show the amount of information to remember.

The process of updating a new cell based on the refined information is as follows

$$C_t = f_t \cdot C_{t-1} + i_t \cdot g_t, \tag{7}$$

where C_t is a memory cell state of current time. If the output value of the f_t is set to zero, the current cell state is determined by the current information. Conversely, if the value of the i_t is set to zero, the current cell state depends only on the cell state at the previous time.

The output decision process using the hidden state and cell state is as follows

$$o_t = \sigma(W_o[h_{t-1}, x_t] + b_o), \tag{8}$$
$$h_t = o_t \cdot \tanh(C_t), \tag{9}$$

where o_t is a output gate composed of W_o and b_o which is weight and bias of output gate. h_t is the new hidden state output.

Finally, prediction of the probability of the clamping force in fully connected layer is performed as:

$$y_{force} = softmax(W_s + b_s), \tag{10}$$

where, y_{force} is the predicted clamping force, W_s is the weights of each gate and b_s is the bias. Figure 8. shows the overall process of the clamping force estimation process.

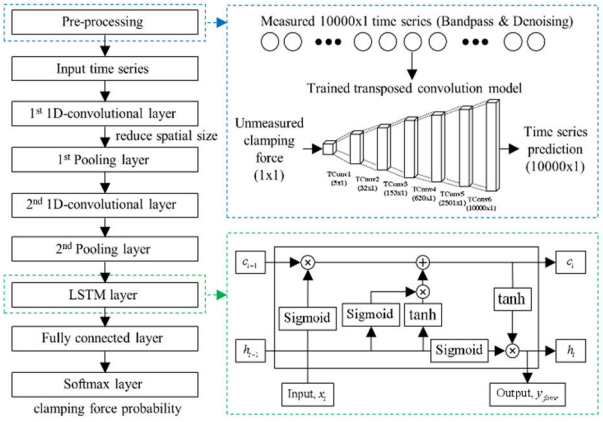

FIGURE 7. The identification process and deep learning layer architecture for clamping force estimation.

IV. CLAMPING FORCE ESTIMATION USING PROPOSED CLSTM

A total of 852 data were used for the training model. The unit of LSTM was 32. A dropout layer with a 25% rate was used after LSTM layer to prevent overfitting. Adam optimizer with learning rate of 0.0001 was used to find the optimal

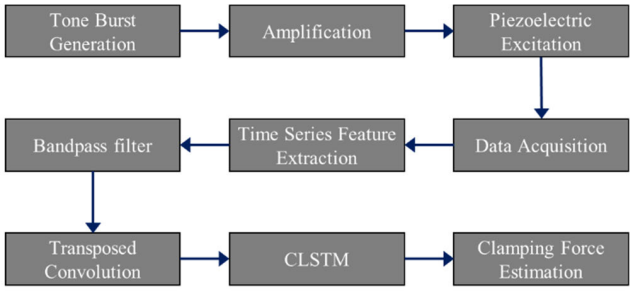

FIGURE 8. Overall process of the proposed clamping force estimation method.

parameters. The mini-batch size of 32 was used for effective memory usage. During training, the accuracy increased and the cross-entropy was decreased. The classification accuracy reached 93.4% and the cross-entropy loss reached 0.28 at 1500 epochs. Figure 9 shows the learning performance of the classifier using the CLSTM algorithm.

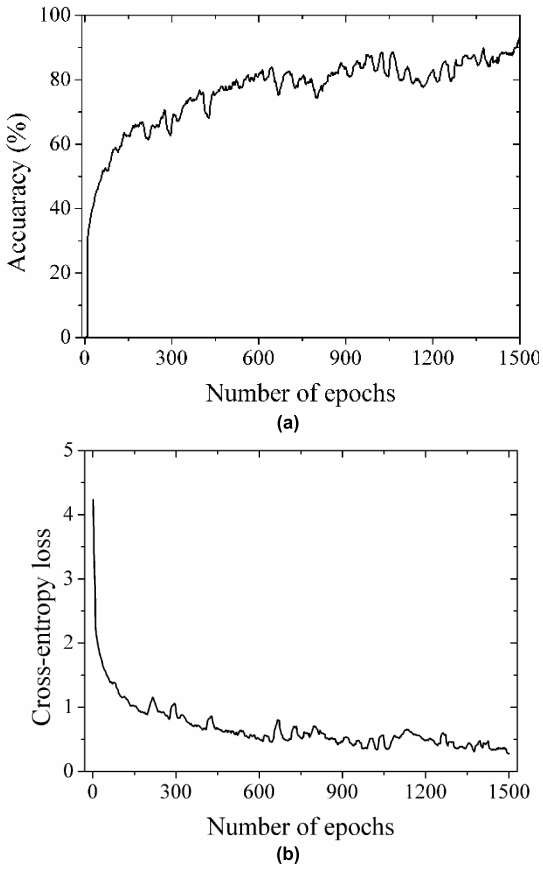

FIGURE 9. Result of the training and validation with increasing number of epochs: (a) accuracy and (b) cross-entropy loss.

The test data were labeled with clamping forces of 0, 10, 20, 30, 40, 50, and 60 kN. Figure 10. shows the prediction result of the CLSTM. Prediction error increased with the increasing clamping force. The mean value for the 10 kN clamping force prediction was 10.25 kN, and the maximum error was 2 kN. The mean value for the 60 kN clamping force was 58.25 kN and the maximum error was 5 kN. At the larger clamping force, the influence on the vibration propagation decreased due to the formation of the fixed constraint. The rate of the magnitude reduction decreased with the increasing clamping force, and affected the prediction accuracy. It is required to apply advanced signal processing methods to distinguish between strong contact conditions. Total error of prediction was 9.13% and the standard variation was 0.04 kN. The proposed methodology showed higher accuracy than the commonly used torque-based method which exhibits estimation errors about 30%. The indirect in-situ estimation of clamping force proposed in this study was possible within errors less than 10%. The increased estimation reliability allows the on-line inspection of the jointed structure in the manufacturing process.

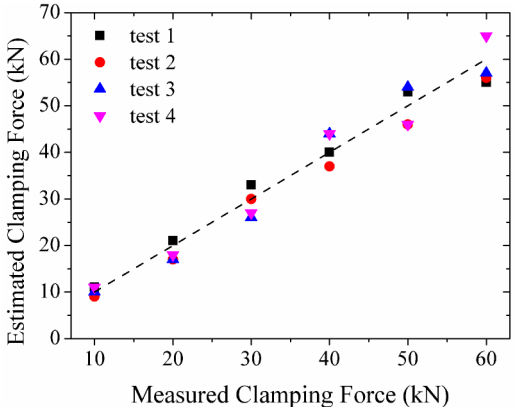

FIGURE 10. LSTM prediction result of clamping force for whole test set.

V. CONCLUSION

In this study, the change of the structural vibration propagation was measured to evaluate the bolt clamping force. An integrated sensing system was designed for achieving vibration excitation and acquisition simultaneously. The sensing system was attached with a constant compressive force. Vibration excitation was implemented by the piezoelectric element and the change in the surface vibration propagation on the wheel structure was confirmed by measurements using attached accelerometer. As the bolt clamping force increased, the wave velocity increased owing to the flexural vibration characteristics. The measured time series data were used for the deep learning to estimate the clamping force. The CLSTM algorithm result shows a high accuracy in evaluating the clamping force. Proposed devise can be utilized in the manufacturing process without any permanent modifications by using detachable equipment. The CLSTM based method allowed accurate identification compared to those achieved using only the tightening torque. The proposed sensing process contributes to the advancement of the real-time inspection of the bolt clamping force in the production process.

REFERENCES

[1] W. A. Grabon, M. Osetek, and T. G. Mathia, "Friction of threaded fasteners," *Tribol. Int.*, vol. 118, pp. 408–420, Feb. 2018, doi: 10.1016/j.triboint.2017.10.014.

[2] T. Fukuoka and T. Takaki, "Mechanical behaviors of bolted joint during tightening using torque control," *JSME Int. J. Ser. A*, vol. 41, no. 2, pp. 185–191, 1998.

[3] T. Fukuoka and T. Takaki, "Evaluations of the tightening process of bolted joint with elastic angle control method," in *Proc. ASME PVP*, vol. 478, 2004, pp. 11–18.

[4] C.-D. Coman and D. M. Constantinescu, "Temperature effects on joint strength and failure modes of hybrid aluminum–composite countersunk bolted joints," *Proc. Inst. Mech. Eng., L, J. Mater., Design Appl.*, vol. 233, no. 11, pp. 2204–2218, Nov. 2019, doi: 10.1177/1464420719837299.

[5] Y. Takao, "Effects of temperature on the response of composite bolted joints," in *Composite Joints and Connections*, L. Tong and P. Camanho, Eds. Cambridge, U.K.: Woodhead, 2011, pp. 295–319.

[6] H.-S. Nah, H.-J. Lee, K.-S. Kim, J.-H. Kim, and W.-B. Kim, "Method for estimating the clamping force of high strength bolts subjected to temperature variation," *Int. J. Steel Struct.*, vol. 9, no. 2, pp. 123–130, 2009.

[7] S. Basava and D. P. Hess, "Bolted joint clamping force variation due to axial vibration," *J. Sound Vibrat.*, vol. 210, no. 2, pp. 255–265, Feb. 1998.

[8] R. Grzejda and A. Parus, "Experimental studies of the process of tightening an asymmetric multi-bolted connection," *IEEE Access*, vol. 9, pp. 47372–47379, 2021, doi: 10.1109/ACCESS.2021.3067956.

[9] R. Miao, R. Shen, S. Zhang, and S. Xue, "A review of bolt tightening force measurement and loosening detection," *Sensors*, vol. 20, no. 11, p. 3165, Jun. 2020, doi: 10.3390/s20113165.

[10] G. Toh, J. Gwon, and J. Park, "Determination of clamping force using bolt vibration responses during the tightening process," *Appl. Sci.*, vol. 9, no. 24, p. 5379, Dec. 2019, doi: 10.3390/app9245379.

[11] S. M. Sah, J. J. Thomsen, M. Brøns, A. Fidlin, and D. Tcherniak, "Estimating bolt tightness using transverse natural frequencies," *J. Sound Vibrat.*, vol. 431, pp. 137–149, Sep. 2018, doi: 10.1016/j.jsv.2018.05.040.

[12] K.-Y. Jhang, H.-H. Quan, J. Ha, and N.-Y. Kim, "Estimation of clamping force in high-tension bolts through ultrasonic velocity measurement," *Ultrasonics*, vol. 44, pp. e1339–e1342, Dec. 2006, doi: 10.1016/j.ultras.2006.05.190.

[13] K. Skrzypkowski, W. Korzeniowski, K. Zagórski, I. Dominik, and K. Lalik, "Fast, non-destructive measurement of roof-bolt loads," *Studia Geotechnica et Mechanica*, vol. 41, no. 2, pp. 93–101, Jun. 2019, doi: 10.2478/sgem-2019-0013.

[14] H. Alhazmi and R. Guldiken, "Quantification of bolt tension by surface acoustic waves: An experimentally verified simulation study," *Acoustics*, vol. 1, no. 4, pp. 794–807, Sep. 2019, doi: 10.3390/acoustics1040046.

[15] X. Jiang, X. Zhang, and Y. Zhang, "Evaluation of characterization indexes and minor looseness identification of flange bolt under noise influence," *IEEE Access*, vol. 8, pp. 157691–157702, 2020, doi: 10.1109/access.2020.3019416.

[16] I. Knight, M. Dodd, C. Grover, R. Bartlett, and T. Brightman, "Heavy vehicle wheel detachment: Frequency of occurrence, current best practice, and potential solutions," Prepared Transp. Technol. Standards, TRL Ltd., Wokingham, U.K., Published Project Rep. PPR086, 2006, vol. 6.

[17] J. D. Varin, "Wheel attachment failures in light-duty vehicles," *J. Failure Anal. Prevention*, vol. 17, no. 4, pp. 660–671, Aug. 2017, doi: 10.1007/s11668-017-0297-0.

[18] A. Dubjansky and M. Bodnar, "Influence of constructive and oscillatory parameters of buses suspension on the road safety," *Ukrainian J. Mech. Eng. Mater. Sci.*, vol. 4, no. 2, pp. 106–114, 2018.

[19] B. Tesfa, G. Horler, F. A. Thobiani, F. Gu, and A. D. Ball, "A clamping force measurement system for monitoring the condition of bolted joints on railway track joints and points," *J. Phys., Conf. Ser.*, vol. 364, May 2012, Art. no. 012021, doi: 10.1088/1742-6596/364/1/012021.

[20] C. Gong, Y. Wang, Y. Peng, W. Ding, M. Lei, Z. Da, and C. Shi, "Three-dimensional coupled hydromechanical analysis of localized joint leakage in segmental tunnel linings," *Tunnelling Underground Space Technol.*, vol. 130, Dec. 2022, Art. no. 104726, doi: 10.1016/j.tust.2022.104726.

[21] C. Yuan, S. Wang, Y. Qi, and Q. Kong, "Automated structural bolt looseness detection using deep learning-based prediction model," *Struct. Control Health Monitor.*, vol. 29, no. 3, Mar. 2022, Art. no. e2899, doi: 10.1002/stc.2899.

[22] Y. Pan, Y. Ma, Y. Dong, Z. Gu, and D. Wang, "A vision-based monitoring method for the looseness of high-strength bolt," *IEEE Trans. Instrum. Meas.*, vol. 70, pp. 1–14, 2021, doi: 10.1109/tim.2021.3101316.

[23] C. Wang, N. Wang, S.-C. Ho, X. Chen, and G. Song, "Design of a new vision-based method for the bolts looseness detection in flange connections," *IEEE Trans. Ind. Electron.*, vol. 67, no. 2, pp. 1366–1375, Feb. 2020, doi: 10.1109/TIE.2019.2899555.

[24] J. Sun, Y. Xie, and X. Cheng, "A fast bolt-loosening detection method of running train's key components based on binocular vision," *IEEE Access*, vol. 7, pp. 32227–32239, 2019, doi: 10.1109/ACCESS.2019.2900056.

[25] A. Bokaian, "Natural frequencies of beams under tensile axial loads," *J. Sound Vibrat.*, vol. 142, no. 3, pp. 481–498, Nov. 1990.

[26] A. Sherstinsky, "Fundamentals of recurrent neural network (RNN) and long short-term memory (LSTM) network," *Phys. D, Nonlinear Phenomena*, vol. 404, Mar. 2020, Art. no. 132306, doi: 10.1016/j.physd.2019.132306.

WANSEUNG KIM received the B.S. degree in mechanical engineering from Hanyang University, in 2018, where he is currently pursuing the Ph.D. degree with the Acoustics and Vibration Laboratory. His research interests include wave analysis, damping materials, fault diagnosis, signal processing, artificial intelligence, and vision.

YEONUK SEONG received the B.S. and Ph.D. degrees in mechanical engineering from Hanyang University, in 2014 and 2021, respectively. His research interests include digital transformation, prediction control, statistical modeling, and deep learning.

JONGSEONG KIM received the B.S. degree from Chungnam National University, in 2014. He is currently an Assistant Manager with Hyundai Motor Group. His research interests include suspension and steering system of vehicle.

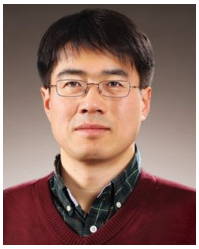

JUNHONG PARK received the B.S. and M.S. degrees from the Korea Advanced Institute of Science and Technology (KAIST), in 1991 and 1993, respectively, and the Ph.D. degree from Purdue University, in 2002. From 1993 to 1998, he worked at Samsung Electronics Company Ltd. He is currently a Professor with the Department of Mechanical Engineering, Hanyang University. His research interests include signal processing, wave analysis, and noise control for improving damping, or machine learning performance, including mechanical issue.